International Journal of Nanomedicine

Dovepress
Taylor & Francis Group

Open Access Full Text Article

ORIGINAL RESEARCH

# Iontophoretic Delivery of Hyaluronic Acid Nanogel-Loaded Fermented Rice Extract Mitigates Skin Glycation

Yuanyuan Han[1,2,*], Yunzhi Lin[3,*], Miao Guo[4], Yinshu Wang[1,2], Xiuju Dong[1,2], Lidan Xiong[1,2], Li Li[1–3], Hua Wang[4], Xuefeng Hu[5,6], Fan Yang[4]

[1]Evaluation Center for Cosmetics Safety and Efficacy, West China Hospital, Sichuan University, Chengdu, Sichuan, People's Republic of China; [2]Sichuan Engineering Technology Research Center of Cosmetic, Chengdu, Sichuan, People's Republic of China; [3]Department of Dermatology, Sichuan University, Chengdu, Sichuan, People's Republic of China; [4]Mageline Biology Tech Co., Ltd, Wuhan, Hubei, People's Republic of China; [5]West China School of Basic Medical Sciences & Forensic Medicine, Sichuan University, Chengdu, Sichuan, People's Republic of China; [6]Rotex Co., Ltd, Chengdu, People's Republic of China

*These authors contributed equally to this work

Correspondence: Xuefeng Hu, West China School of Basic Medical Sciences & Forensic Medicine, Sichuan University, No. 17, Section 3, People's South Road, Chengdu, 610000, People's Republic of China, Email huxuefeng@scu.edu.cn; Fan Yang, Mageline Biology Tech Co, Ltd, Han Street, Wuchang District, Wuhan, Hubei, 430060, People's Republic of China, Email yangfanfenix@outlook.com



**Purpose:** This study aims to evaluate the efficacy of Saccharomyces/Rice Ferment Filtrate (SRFF) in mitigating glycation-related skin aging, specifically focusing on the reduction of advanced glycation end products (AGEs) through improved transdermal delivery using nanotechnology and iontophoresis.

**Methods:** We developed a hyaluronic acid (HA) nanogel as a carrier for SRFF, which enhances drug delivery efficiency and stability while providing skin protection. Iontophoresis, a non-invasive electrochemical method, was employed to facilitate the transdermal penetration of SRFF into the skin. An ex vivo skin tissue glycation model was established, and immunohistochemistry and tissue mechanics assessments were conducted to analyze the effects of SRFF combined with HA nanogel and iontophoresis.

**Results:** The combination of SRFF with HA nanogel and iontophoresis significantly reduced the formation of AGEs and mitigated the stiffening effects associated with glycation. The results demonstrated pronounced anti-glycation effects at both the cellular and ex vivo tissue levels. The observed reductions in AGEs and improved skin barrier functionality were likely due to the antioxidant properties of SRFF and its ability to competitively bind to AGEs crosslinking sites.

**Conclusion:** This study highlights the potential of SRFF, in conjunction with HA nanogels and iontophoresis, as an effective method for anti-glycation treatment, reducing AGE accumulation and alleviating skin yellowing and stiffness. The findings support the development of non-invasive, efficacious strategies for enhancing skin health and counteracting the effects of aging.

**Keywords:** advanced glycation end products, natural inhibitors, non-invasive transdermal, flexible electrodes, mechanical characterization of skin

## Introduction

Skin glycation is an inherent biochemical process that results in the formation of advanced glycation end products (AGEs), which accumulate in the body after their production. The formation of AGEs is a gradual process that starts with the reaction between a carbonyl group from a reducing sugar and an amine group from amino residues (such as lysine or arginine) on proteins or lipids. This initial reaction generates intermediates, which can subsequently react to produce AGEs.[1,2] The increased formation of AGEs typically occurs alongside elevated or dysregulated levels of reactive oxygen species (ROS).[3] AGEs mediate a series of signaling pathways that affect cell apoptosis and differentiation, ultimately leading to structural damage in tissues.[4,5] AGEs have been shown to be associated with various dermatological conditions and the aging process.[6,7] In the dermis, AGEs cross-link with collagen, causing protein browning and fiber

Received: 26 February 2025
Accepted: 7 September 2025
Published: 18 September 2025

**Graphical Abstract**

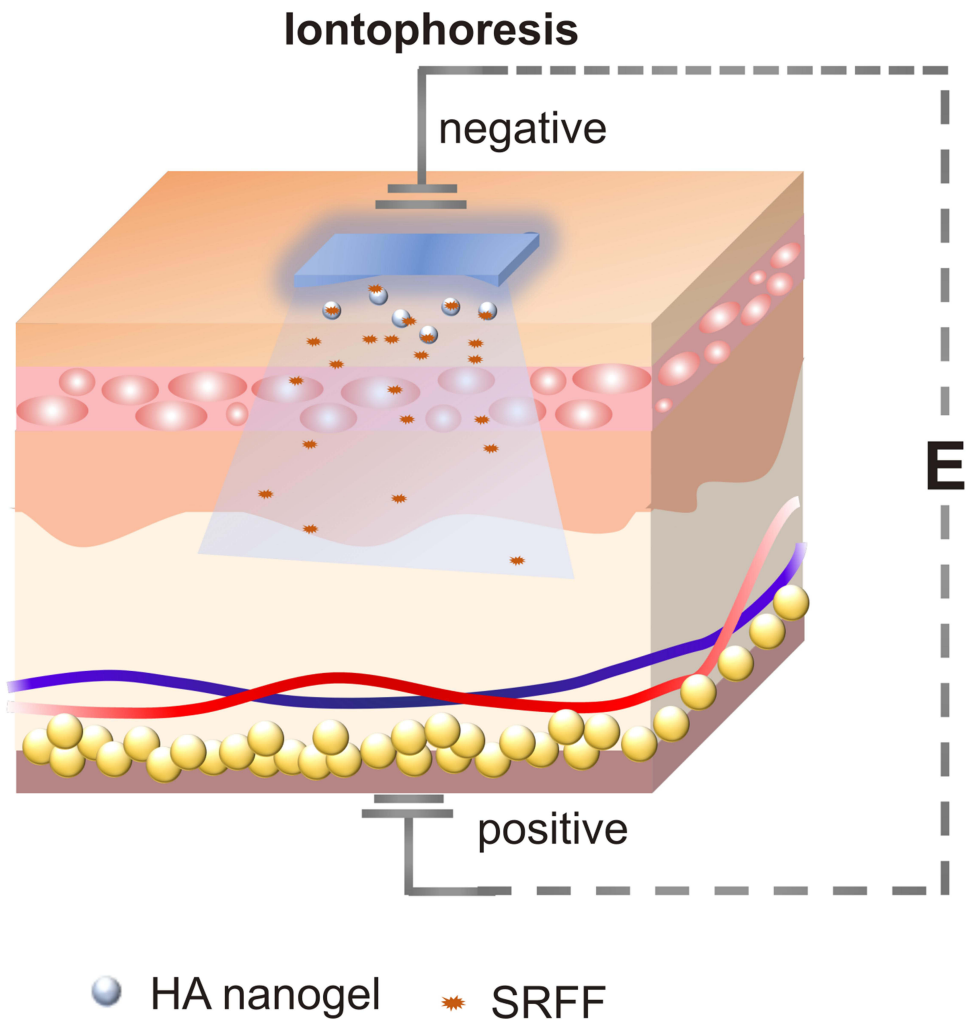


deformation. Glycated elastin fibers become thinner and lose their elasticity, resulting in skin that appears dull, yellow, rough, and increasingly prone to wrinkles.[8,9] Strategies aimed at reducing glycation could lead to significant improvements in skin appearance and overall health.

Reducing the accumulation of AGEs can be directly achieved by decreasing the intake of sugars and exogenous AGEs. It has been shown that low-sugar diets can lower sugar levels in the skin. Conversely, a careful diet is only preventive and cannot reverse AGEs and protein crosslinks.[10] Treatment methods such as radiofrequency[11] and microneedling[12] can be employed to reduce the expression of AGEs and ameliorate the symptoms of skin glycation. These methods are generally complex, require administration in specialized medical facilities, and their underlying mechanisms are not yet fully understood. In particular, the use of microneedles carries a risk of infection when they puncture the skin.[13]

Currently, various therapeutic agents targeting AGEs inhibit their formation by removing free radicals, chelating metal ions, capturing dicarbonyl compounds, and disrupting the covalent crosslinks with AGEs.[14] For example, metformin can enhance the activity of glyoxalase I (GLO1), thereby reducing the levels of methylglyoxal, an important precursor of AGEs, finally leading to a decrease in AGEs expression levels.[15] Aminoguanidine, on the other hand, is a prototypical therapeutic agent that reacts rapidly with α,β-dicarbonyl compounds to block AGEs formation.[16]

Unfortunately, synthetic AGEs inhibitors may pose safety concerns and cause side effects.[17,18] This highlights the promising outlook for developing natural compounds with low toxicity that exhibit anti-glycation activity in the skin.[19] These natural components, which show potential in inhibiting the formation of AGEs, include polyphenols, polysaccharides, vitamins, alkaloids, and peptides.[20–22] For instance, cranberry juice polyphenols and their fractions can scavenge reactive carbonyl groups and form neoadducts that effectively inhibit collagen glycation and disrupt AGEs induced collagen cross-linking.[21] Moreover, supramolecular carnosine can inhibit the expression of the receptor for AGEs (RAGE) and reduce AGE levels by upregulating Nrf2 protein expression and enhancing antioxidant defense mechanisms in melanocytes.[22]

When using medicines for dermatological treatment, topical medications provide more effective options than systemic administration due to their numerous advantages, including targeted delivery, minimized systemic side effects, and enhanced bioavailability.[23] However, natural inhibitors, particularly peptides, polyphenols, and polysaccharides, are primarily hydrophilic, which hinders effective transdermal absorption when applied topically. Therefore, it is necessary to explore suitable transdermal enhancement technologies to improve drug permeation rates and enhance therapeutic effects.

To address the challenges of efficiently and safely delivering hydrophilic substances through the skin, iontophoresis presents a promising solution. Iontophoresis is a non-invasive technique that utilizes electrochemical methods to introduce medications into the deeper layers of the skin. This process involves stimulating the skin surface with an electric field, which opens cellular channels and increases the permeability of cell membranes, thereby facilitating the transdermal passage of ions or molecules.[24,25] In traditional iontophoresis, the most commonly used electrodes are Ag/AgCl electrodes. However, they can cause precipitation of insoluble silver chloride at the anodal surface during the process. Rigid stainless-steel electrodes lack sufficient flexibility and have high chemical reactivity, leading to the leaching of iron ions and resulting in potential toxicity. To overcome these limitations, we have developed a flexible electronic skin mask delivery system. This system employs titanium composited with polyethylene glycol terephthalate (PET) as the electrode material. Titanium is less reactive, ensuring that it does not release metal ions. Additionally, the elastic modulus of this type of electrode closely matches that of human skin, allowing for good conformity and contact with complex body contours. This design ensures highly efficient and safe transdermal delivery of therapeutic agents, which has been reported in our previous study.[26]

In this study, we selected natural extracts Saccharomyces/rice ferment filtrate (SRFF), which is a type of rice extract fermented with specific strains of the yeast Saccharomyces, as the active ingredient due to its effectiveness in combating aging and enhancing the skin barrier.[27,28] Directly applying the SRFF solution between the electrode and the skin can result in uneven contact and difficulties in retention, which may limit the drug delivery efficacy. Therefore, a hyaluronic acid (HA) nanogel is prepared to serve as a medium for delivering SRFF, enhancing delivery efficiency, stability, and providing adequate skin protection. The combination of nanogels and iontophoresis is expected to enhance the effectiveness of SRFF in reducing the accumulation of AGEs and combating skin glycation.

# Materials and Methods

## Analysis of SRFF Components

The composition of SRFF (Mageline Biology Tech Co., Wuhan, China) was identified using a high-performance liquid chromatography-mass spectrometry (HPLC-MS) platform (Thermo Fisher Scientific Inc., Ultimate 3000LC, Q Exactive HF, Waltham, USA), and the chromatographic column was C18. The chromatographic separation conditions were as follows: column temperature 30 °C; flow rate 0.3 mL/min; mobile phases composed of A: water + 0.1% formic acid and B: pure acetonitrile. The HPLC elution conditions are detailed in Table S1. Measurements were performed twice.

## HA Nanogels Synthesis

The preparation process refers to the previous report.[29]

Modification: 1 g of enzyme-cut sodium HA (Mw<10k Da, Aladdin, Shanghai, China) and 1 mL of methacrylic anhydride (MA, $C_8H_{10}O_3$, Maklin, Shanghai, China) were dissolved in 100 mL of deionized water, stirred in an ice-water

bath, and the pH of the mixture was adjusted to approximately 8. After 24 hours of reaction, the mixture was dialyzed and lyophilized to MAHA powder.

The dialysis conditions for HAMA purification: dialysis was performed at room temperature in ultrapure water at pH 7, with a volume 20 times that of the reaction solution. The dialysis membrane used was regenerated cellulose with a glycerol coating, and a molecular weight cut-off (MWCO) of 3500 Da (Solarbio, model MD55). The dialysis membrane was boiled prior to use. Dialysis lasted for 72 hours, with four water changes; the first exchange occurred 6 hours after the start of dialysis.

Lyophilization process: the dialyzed solution was frozen overnight at −80°C. Subsequently, freeze-drying was performed using a freeze dryer (LC-10N-60A, Lichen, China). The freeze-drying conditions included a condenser temperature of approximately −60°C, a sample shelf temperature of −10°C, continuous vacuum pumping at a pressure of approximately 5–20 Pa, for about 24 hours. The entire lyophilization process was performed protecting the samples from light to maintain stability.

Three NMR peaks located at 6.1, 5.6, and 1.8 ppm corresponding to the hydrogen atoms of methylene (a, b) and methyl (c), respectively, demonstrated that methacrylic acid was successfully modified on HA, and the degree of substitution was about 10%. (shown as in Figure S1).

Gelation: 50 mg of MAHA was dissolved in 10 mL of aqueous solution and crosslinked with 63 mg di(ethylene glycol) diacrylate (DEGDA, Maklin, Shanghai, China). 0.1 g of potassium persulfate (K2S2O8, Maklin, Shanghai, China) was added as a thermal initiator at 70°C to initiate crosslinking and form nanogels. The molar ratio of MAHA to DEGDA was calculated to be approximately 1:127.2, and the thermal initiator concentration was 10 mg/mL (approximately 0.0370 M).

Fluorescent labeling: 100 mg of MAHA in deionized water and fluorescein 5-isothiocyanate (FITC, Sigma-Aldrich, Saint Louis, USA) in 0.25 mL of Dimethyl sulfoxide (DMSO, Aladdin, Shanghai, China) reacted overnight at room temperature under light protection. Then the mixture was precipitated in a large amount of anhydrous ethanol to obtain FITC-labeled HAMA, which was used to prepare fluorescent labeled HA nanogels.

## HA Nanogels Characterization

The degree of methacrylic acid substitution was determined by nuclear magnetic resonance spectroscopy (NMR, Bruker 400MHz, Billerica, USA). The particle size of HA nanogels was characterized using scanning electron microscope (SEM, JEOL JSM-IT700HR, Tokyo, Japan). The nanogel particle size distribution and Zeta-potential was analyzed by a dynamic light scattering (DLS) with a Zeta-potential analyzer (HORIBA SZ-100, Kyoto, Japan).

## SRFF Loading and Release From HA Nanogels

The SRFF-loaded nanogels (SRFF@nanogel) were prepared by co-dispersing HA nanogel (10 mg) lyophilized powder with SRFF solution (10 mg/mL), and the mixture was stirred overnight at room temperature, to allow SRFF to equilibrate between the aqueous phase and the nanogel. The unloaded SRFF was then removed by centrifugation. The SRFF@HA nanogels obtained in the previous step were placed in dialysis bags (MWCO = 3500 Da). They were then immersed in PBS solution (pH 7.4) at 37°C under gentle stirring. At predetermined time intervals, aliquots of the external PBS solution were withdrawn to measure the amount of released free SRFF. The concentration of SRFF was determined by measuring absorbance at 270 nm using UV-visible spectroscopy (Thermo, Scientific Multiskan Sky, Waltham, USA). The absorbance values were then converted to concentration using a previously established standard curve (Figure S2). The release profile was plotted as cumulative SRFF release (%) versus time. To maintain sink conditions, the withdrawn aliquots were immediately replaced with an equal volume of fresh PBS solution. The release curve measurement was performed three times. The UV-visible absorption spectroscopy method used to determine SRFF release was based on previously reported studies.[29,30]

## Anti-Glycation Effect of SRFF on Fibroblasts

Fibroblasts were seeded in 96-well plates at a density of 10,000 cells per well and treated with DL-glyceraldehyde (GLA, Sigma-Aldrich, Saint Louis, USA) at varying concentrations (5, 1.25, 0.3125, and 0 mM) for 24 hours. The CCK-8 assay

(Dojindo Laboratories, CK04, Kumamoto, Japan) was then employed to evaluate cell proliferation and determine safe concentrations for the use of GLA. The anti-glycation effect of SRFF was evaluated by adding solutions of 10 mg/mL and 1 mg/mL to glycation-affected cells.

## Efficacy and Safety Evaluation of Iontophoresis

Iontophoresis was performed using the Transdermal Drug Delivery System (Rotex Inc, Chengdu, China), under the following conditions: current density 0.6 mA/cm$^2$, and duration of 25 minutes. The negative electrode was connected to a hydrogel loaded with drugs, and the positive electrode was connected to ex vivo skin tissue.

This study utilized ex vivo skin tissue sourced from discarded foreskin samples of six young, healthy patients aged 6 to 10 years. The skin color was classified as Type II according to the Fitzpatrick skin type classification. The samples were collected from the Dermatology outpatient clinic and the Pediatric Surgery operating room at West China Hospital. Informed consent was obtained from all volunteers prior to their participation, ensuring they were fully informed about the purpose, nature, and potential risks associated with the study. The research protocol was conducted in accordance with the principles of the Declaration of Helsinki and approved by the West China Hospital Ethics Committee (Approval No.: 2024(2292)), in accordance with ethical requirements. All procedures were carried out in compliance with relevant ethical standards.

To determine the efficacy of iontophoresis, SRFF solution was delivered onto ex vivo skin tissue. Next, the skin surface was repeatedly stripped with adhesive tape to remove the epidermal layer. Then the flavonoid content was then tested. Specifically, rutin, a plant-derived flavonoid-rich compound,[31] was used as the standard. When aluminum chloride reagent is added to the flavonoid methanol solution, flavonoid groups such as 3-, 4-, 5-hydroxyl, 4-carbonyl, and ortho-dihydroxyl moieties complex with $Al^{3+}$ ions. Under alkaline conditions, a red complex forms that can be measured at 510 nm. Within a certain concentration range, absorbance at 510 nm correlates highly with flavonoid concentration. This is a classical method for flavonoid quantification.[32]

The safety evaluation experiments consisted of two groups: the blank group (no treatment) and the iontophoresis group. The tissues collected at 24 hour and 72 hours, respectively, with three replicate samples in each group. The tissues were stained with Ki67 (Huabio, HA721115, Wuhan, China) and CD3 (eBioscience™, 14–0037-82, San Diego, USA) to determine whether the iontophoresis would affect the viability of the tissues.

## Epidermal Residency Effect

6-week-old C57BL/6J mice (SPF Beijing Biotechnology Co., Ltd. Beijing, China) were shaved, and fluorescently labeled nanogels were iontophoresed on the back for 25 minutes, and then the nanogels were wiped off the surface. Fluorescence imaging was performed using a small animal in vivo imaging system (IVIS, PerkinElmer IVIS Lumina III, Waltham, USA). The painted gel group was used as a control. Fluorescence imaging was performed again on the fifth day thereafter. This study was conducted in accordance with ethical standards for animal research. All procedures involving mice were approved by the Animal Ethics Committee of West China Hospital (Approval No.: 20240228047) in accordance with the Guidelines for Welfare and Ethical Review of Laboratory Animals (China, GB/T 35892–2018), with additional reference to international consensus guidelines (IAVE Guidelines, 2010) to ensure animal welfare. The experiments were designed to minimize the number of animals used and to reduce any pain or distress experienced by the animals. All animals were housed under standard laboratory conditions with access to food and water, and every effort was made to ensure humane treatment throughout the study.

## Skin Glycation Model Establishment and Treatment

The GLA (40 mM) was used to induce the glycation. The groups were as follows: the blank group without treatment, the other groups treated with GLA for 24 hours. Then the painting group and iontophoresis group were treated with SRFF (10 mg/mL) via different drug delivery methods, ie, painting and iontophoresis, respectively. The b* value, which represents the blue-yellow chroma of skin was measured at different time points to track changes in skin tissue color.

### H&E Staining and Immunohistochemistry/Immunofluorescence

For H&E staining, tissue sections were first stained with hematoxylin, which binds to nuclei and stains them blue. Then eosin was used to stain cytoplasm and extracellular structures pink. Immunohistochemical staining was performed using the anti-AGE antibody (Abcam, ab23722, Boston, USA) and the anti-carboxymethyl lysine antibody [CML26] (Abcam, ab125145, Boston, USA). Immunofluorescence was also performed using anti-carboxymethyl lysine antibody [CML26].

### Mechanical Characterization

Texture Analyzer: The instrument used was the TA.XTC-20 Texture Analyzer (TA Instruments, Guangzhou, China). The sample area was approximately 0.6 $cm^2$, with a uniform, smooth surface free of impurities. Set experimental parameters, including the predefined compression speed (0.01 mm/s), compression distance or stress, and maximum strain (20%). The instrument's compression head would apply force at the set speed to collect force-displacement or force-time data. To ensure data reliability, multiple samples were tested repeatedly.

Atomic force microscope (AFM): Frozen sections of skin tissue with a thickness of 8 μm, were analyzed using an AFM (Shimadzu, SPM-Nanoa, Tokyo, Japan). The mechanical module operated in contact mode to determine the elastic modulus of the skin tissue. The probe used was the CSG30, with a spring constant of 0.6 N/m, and a tip radius of 10 nm made of silicon. Testing conditions included a pixel resolution of 128 × 128, a scan area of 1×1 μm, and a scanning speed of 8.0 Hz.

## Statistical Analysis

Statistical figures were generated using GraphPad Prism software (version 9.5). Statistical significance for all experiments was determined using Student's t-tests unless otherwise specified. A p-value $\leq 0.05$ was considered statistically significant. For the ex vivo skin studies, skin samples were selected to match thickness and color. The sample size was determined based on standard biological experimental criteria, ensuring both intergroup and intragroup replicates with $n \geq 3$.

# Results

## Comprehensive Analysis of the Full Ingredients of SRFF

Based on the HPLC-MS analysis, SRFF was found to contain over 130 active components, predominantly comprising amino acids and peptides, nucleotides and adenosine, fatty acids, flavonoids, polyphenols, retinoic acid, ceramides, and glycerophospholipids, as shown in Figure 1a. Among these constituents, amino acids and peptides constitute the majority at 60.08%. Next are nucleotides and adenosine, accounting for 29.80% of the composition. Flavonoids and polyphenols constitute 3.44% of SRFF. Additionally, fatty acyls (2.02%), glycerophospholipids (0.62%), and ceramides (0.21%) were also found.

## Preparation and Characterization of HA Nanogels

The synthesis pathway of nano-hydrogels, as shown in Figure 1b, involves two steps: the first is the modification of the HA side chains with methacrylic acid groups, with the NMR spectra are presented in Figure S1. The second step involves the crosslinking of MAHA with the initiator. Due to the low concentration of polymers used, the products formed well-dispersed nano-hydrogel particles instead of bulk hydrogels.

The particle size of nano-hydrogels was determined using both SEM and DLS analysis. The diameter measured by SEM was approximately 55 nm (Figure 1c). The size measured by DLS was 91.9±1.4 nm, and zeta potential was −12.2 ±1.2 mV (Figure 1d and Table S2). Since DLS measures the hydrodynamic radius, the size obtained is slightly larger than that measured by SEM.

## The Sustained Release and Retention Effect of SRFF@HA Nanogel

Using HA nanogel for loading SRFF, the drug loading amount was determined to be 3.0 mg per 10 mg (SRFF mass/SRFF@HA nanogel mass), which was calculated based on the absorption intensity from UV-Visible spectroscopy. We also compared the particle size and zeta potential of the HA nanogel before and after loading with SRFF. The particle

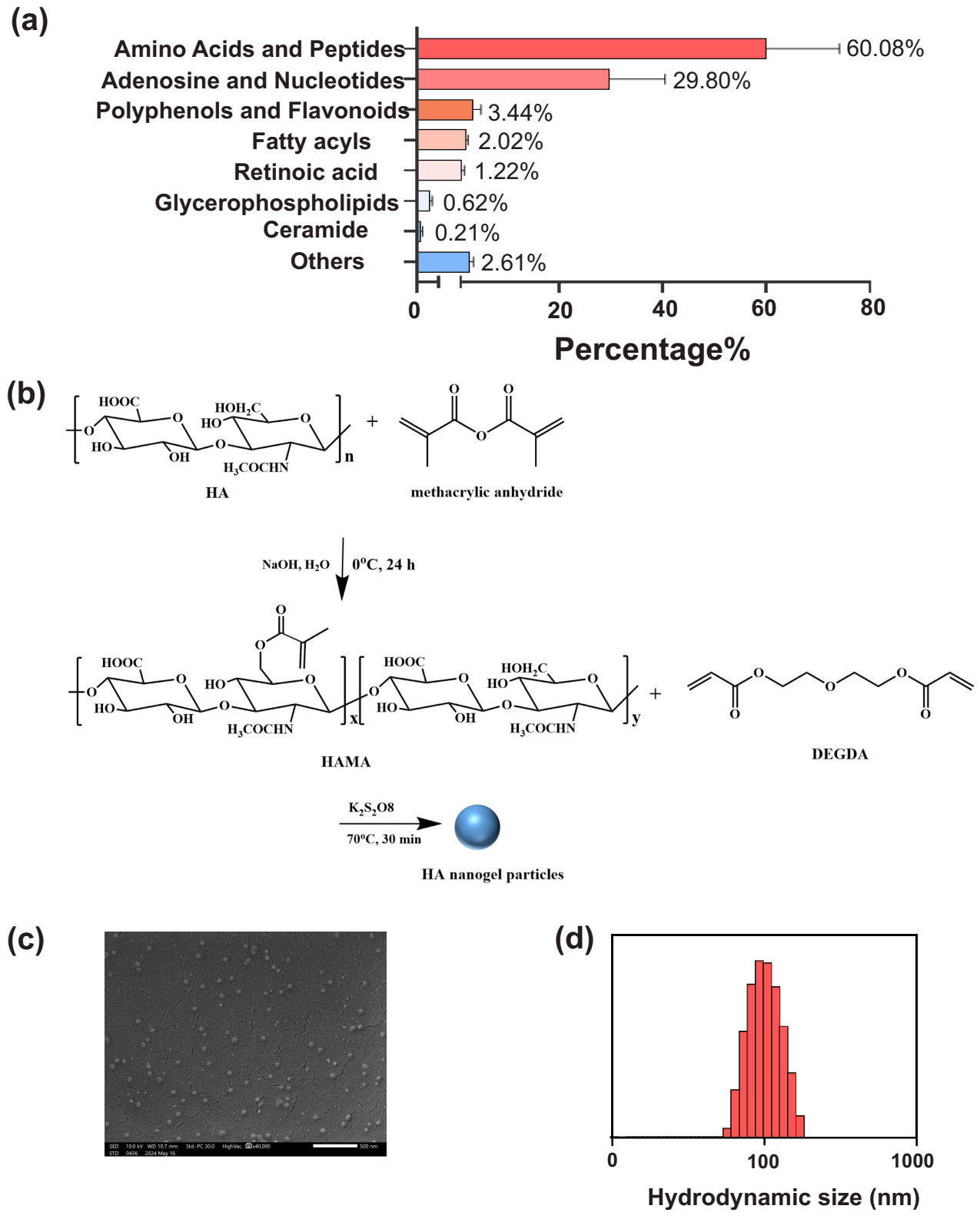


**Figure 1** Analysis of the components of the SRFF and the synthesis of its nanocarrier. (**a**) Full ingredients of SRFF analysis. (**b**) Schematic illustration of HA nanogel preparation process. (**c**) Representative SEM image of dispersed HA nanogel particles. (**d**) The hydrodynamic size distribution of HA nanogels measured by DLS (Repeated three times, and the image shows the result from one of those trials).


https://doi.org/10.2147/IJN.S523731

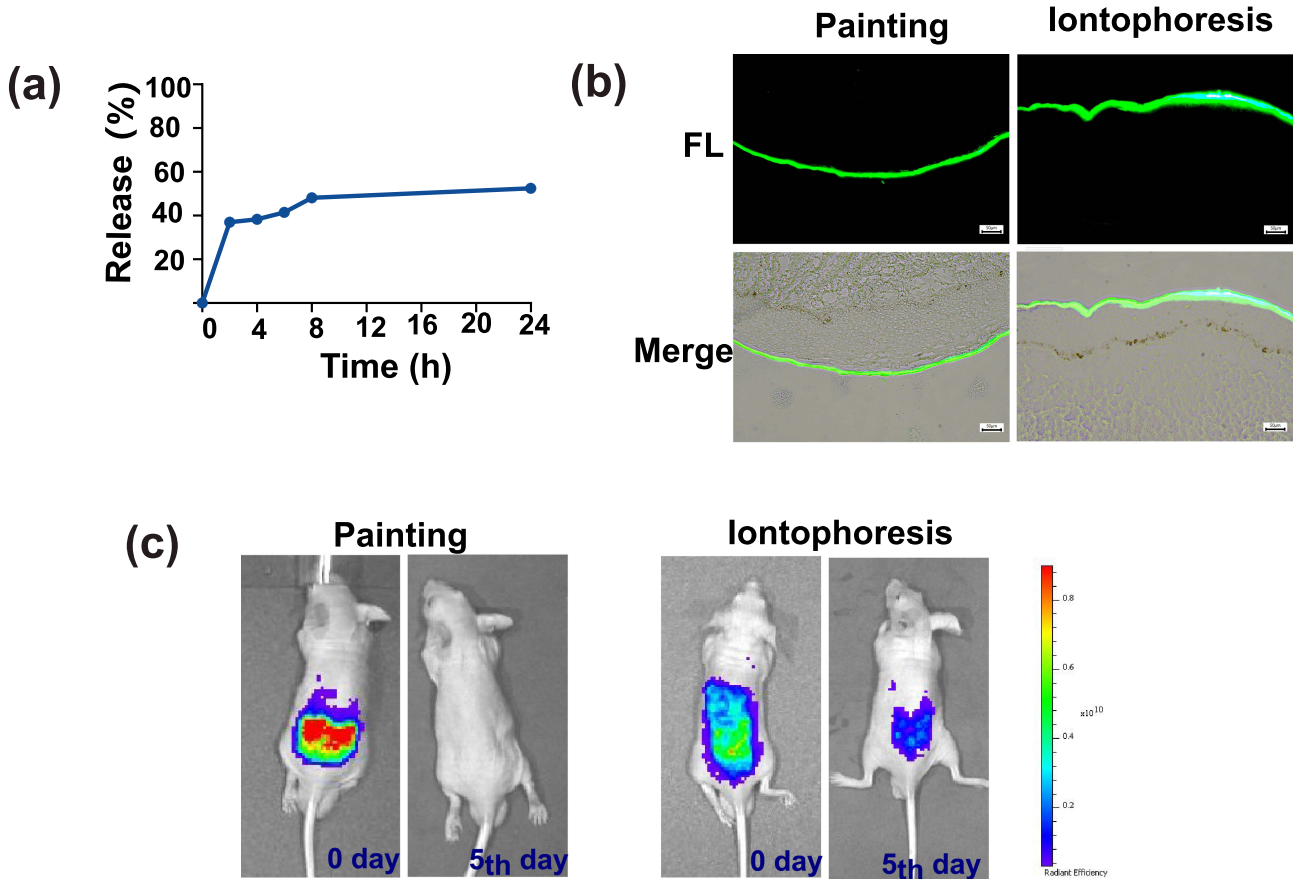


**Figure 2** The sustained release and retention properties of SRFF@HA nanogel. (**a**) Release curve of SRFF encapsulated in HA nanogels. (**b**)Fluorescence images of FITC-labeled nanogels used via and painting and iontophoresis method, scale bar = 50 μm. (**c**) Live fluorescence images of painting group and the iontophoresis group at 0 day and 5th day.

size showed no significant change following the loading process. In terms of zeta potential, the values shifted from −12.2 ± 1.2 mV prior to loading to −7.1 ± 1.6 mV post-loading, indicating a reduction in the magnitude of the negative surface charge. Detailed data are provided in Table S2.

The release of SRFF from SRFF@HA nanogel was monitored at different time points to plot the release profile, as shown in Figure 2a. Approximately 36.9% of SRFF was released within the initial 2 hours, possibly due to the physical loading of SRFF onto the nanogels with loose binding, facilitating faster release. Subsequently, a slow release was observed as the nanogels swelled, with approximately 52.4% released in 24 hours.

Next, FITC-labeled nanogels were topically applied or via iontophoresis to assess their penetration into the epidermis. Fluorescence imaging showed that nanogels in both methods reached the epidermal layer, but both of them did not penetrate further, as shown in Figure 2b. Thus, the study questioned whether nanogels applied via iontophoresis persist longer than those applied topically. To address this issue, FITC-labeled nanogels were detected using an in vivo imaging system in fluorescence imaging mode. Immediately after application of SRFF@HA nanogel, strong FITC fluorescence signals were observed on the backs of mice in both the painting group and the iontophoresis group, confirming the presence of nanogels on or within the skin. However, after 5 days, the FITC signal disappeared in the painting group, whereas it remained clearly detectable in the iontophoresis group (Figure 2c). This suggests that nanogels stay longer after iontophoresis, facilitating the residence and sustained release of the loaded SRFF.

## The Iontophoresis Enhances the Transdermal Absorption Safely and Efficiently

The skin tissues were cultured for 72 hours post-iontophoretic permeation, and Ki67 and CD3 immunostaining were used to evaluate safety. As shown in Figure S3a and S3b, Ki67 expression in the tissues remained consistent at both 24 and

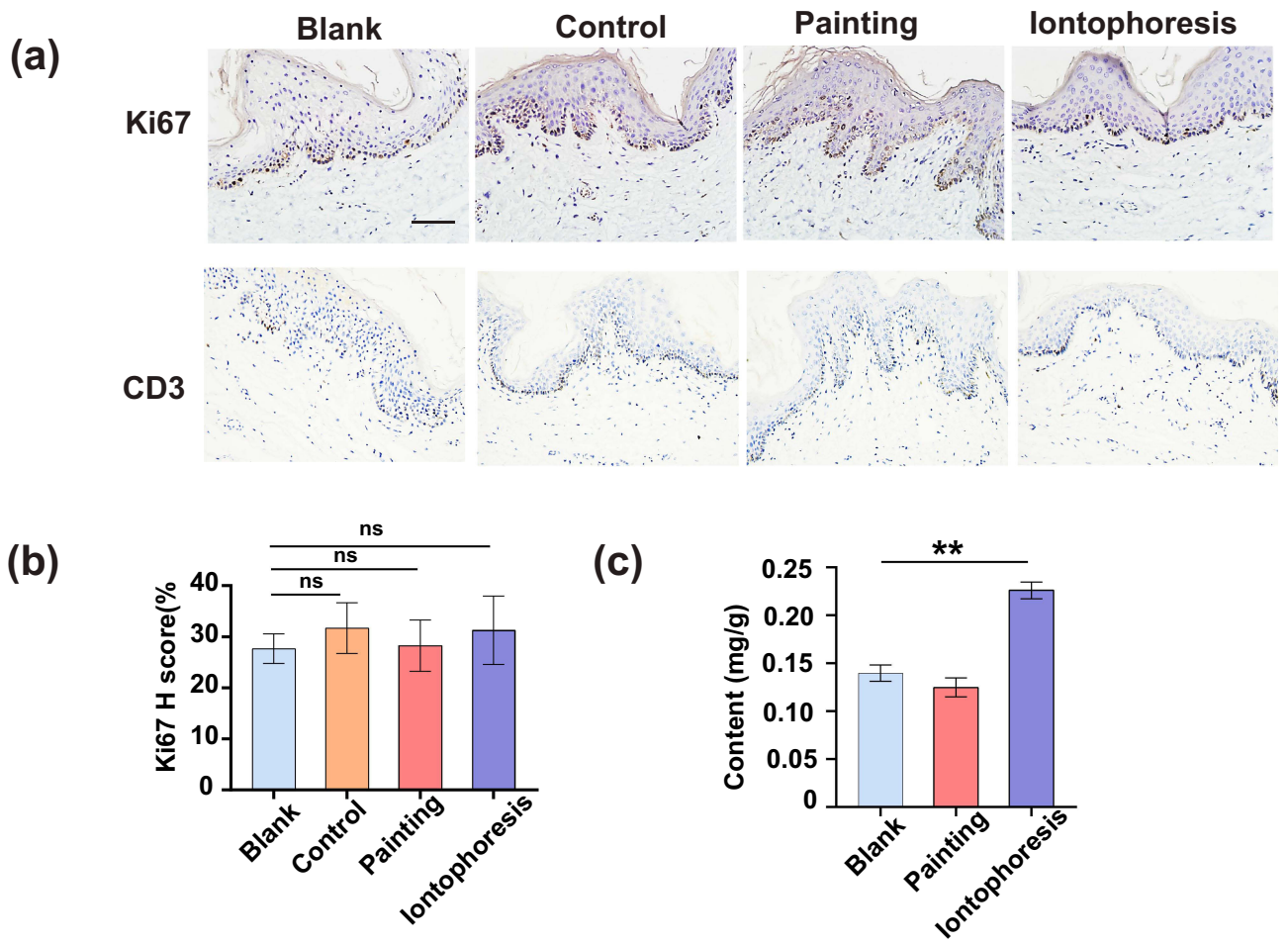


**Figure 3** Evaluation of the safety and transdermal permeability of ion infusion. (**a**) Images of Ki67 and CD3 IHC stained skin tissues from different groups (scale bar represents 50 μm). (**b**) Ki67 score of the different groups (ns represents $P>0.05$ compared with the blank group). (**c**) The content of flavonoid in different groups (** represents $P<0.01$ compared with the blank group).

72 hours after iontophoresis. In Figure 3a and b, there were also no significant difference in Ki67 expression between iontophoresis-treated and untreated samples, indicating that iontophoresis did not affect tissue vitality. After iontophoresis, CD3 was also not expressed in the skin tissue, indicating that the treatment did not activate the skin's immune response.

Subsequently, we introduced SRFF into skin tissues to assess if iontophoresis enhances transdermal absorption. The content of flavonoids, an important antioxidant component in SRFF, served as an indicator since human skin lacks plant-derived flavonoids, eliminating intrinsic tissue effects. Following painting and iontophoresis, the stratum corneum was removed with tape stripping to eliminate the influence of SRFF adhering to the skin surface. The results revealed the iontophoresis group notably detected flavonoid compounds at a content of 0.2260±0.0087 mg/g (flavonoid compound mass/tissue mass, Figure 3c), demonstrating statistical differences ($P<0.01$) compared to the painting group and the blank control group. These results suggest that SRFF penetrated the stratum corneum after iontophoresis, facilitating transdermal absorption, thus presenting a method suitable for subsequent experiments.

Based on these results, iontophoresis of SRFF was found to allow it to penetrate the epidermal layer and reach the dermal layer, while nanogels facilitated its residence in the epidermal layer for slow release. Therefore, for future use, a mixture of SRFF solution and SRFF@HA nanogel will be utilized. This approach will allow some free SRFF to be directly imported to exert its effects, while the portion encapsulated in nanogels will be released slowly, providing prolonged activity.


https://doi.org/10.2147/IJN.S523731

## AGEs and CML in Skin Cells and ex-vivo Skin Tissues Can Be Activated by GLA

GLA has been shown to promote glycation through the formation of AGEs and CML in various organs, such as the skin, liver, and kidneys.[33] To assess the sensitivity of AGEs to GLA in fibroblasts and ex vivo skin tissues, varying concentrations of GLA were administered to the cells and tissues, followed by immunohistochemical analysis using anti-AGE and anti-CML antibodies. In alignment with previously published findings,[33,34] an increase in CML staining was observed in fibroblasts, along with detectable staining for AGEs and CML in ex vivo tissues (Figure 4a–d). Simultaneously, an increase in yellowness was both visually and quantitatively detected using a colorimeter, suggesting that glycation of the epidermal skin contributes to the manifestation of skin yellowing. Notably, we observed the onset of tissue rigidity and hardening through sensory perception. Consequently, we have preliminarily investigated the evaluation of skin glycation levels by examining the mechanical properties of the tissue (Figure 4e and f).

GLA was used to induce glycation in fibroblasts, and CCK-8 assay results indicated that GLA concentrations below 1.25 mM were found to be non-toxic to fibroblasts (Figure S3c). Therefore, we chose 1.25 mM (high concentration, HC) and 0.3125 mM (low concentration, LC) as the concentrations for establishing the glycation model. Fibroblasts were

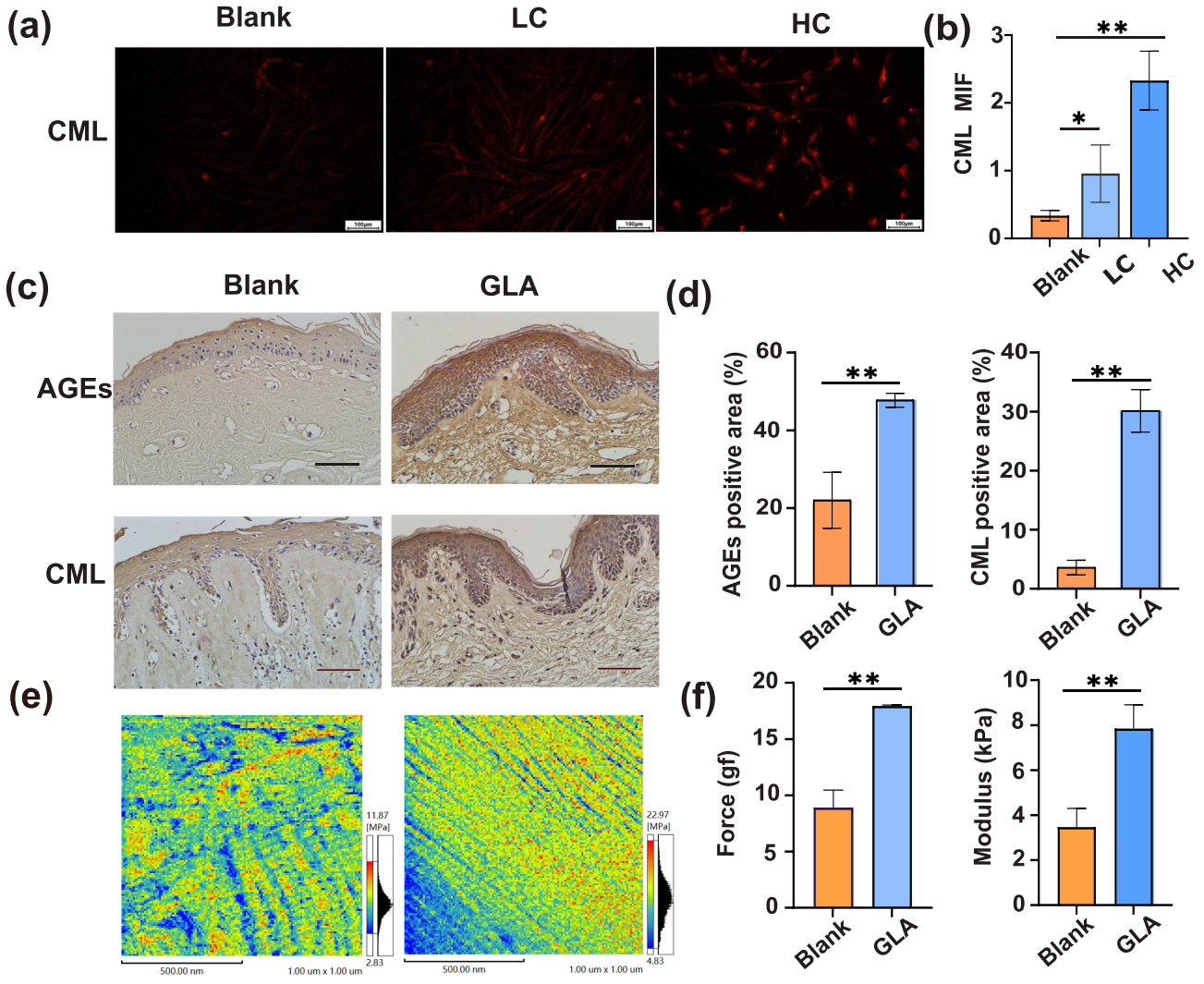


**Figure 4** The GLA induced glycation of cells and skin tissues. (**a**) CML (red) stained fibroblasts treated by 1.25 mM (HC) and 0.3125 mM (LC) GLA solution (scale bar = 50 μm), and (**b**) relatively quantitative comparison between the blank group and treated groups (* and ** represents $P$ <0.05 and $P$ <0.01 compared with the blank group, respectively). (**c**) AGEs and CML immunohistochemistry staining area comparison among blank and GLA treated group. Scale bar is 50 μm. (**d**) Relative quantification of dermal area occupied by AGEs and CML positive staining (** represents $P$ <0.01 compared with the blank group). (**e**) Elastic modulus maps of blank (left) and GLA treated (right) sample obtained by AFM (scale bar is 500 nm). (**f**) The forces to achieve 20% strain and Young's modulus comparison between samples with and without GLA treatment (** represents $P$ <0.01 compared with the blank group).

subsequently treated with both HC and LC GLA, and the results showed that both concentrations significantly increased the expression of CML. Notably, the HC condition resulted in a higher level of CML expression.

Similarly, GLA at 40 mM was used to induce glycation in ex vivo skin tissue, significantly increasing AGEs and CML expression compared to the blank group ($P<0.01$), as shown in Figure 4c and d. CML is widely recognized as a marker for AGEs, which accumulates during skin aging and glycation processes. Its levels can directly reflect the extent of glycation within the tissue, making CML measurement an effective method for assessing the efficacy of anti-glycation interventions. Consequently, CML was selected as the glycation marker to evaluate the anti-glycation effects of SRFF.

Glycation leads to increased collagen cross-linking, which affects the structure and elasticity of the extracellular matrix (ECM) in both the dermis and epidermis, significantly impacting the mechanical properties of the skin. Therefore, a comparison of mechanical properties before and after glycation was conducted. AFM-based indentation revealed that the Young's modulus increased from 6.44 MPa to 13.22 MPa post-glycation (Figure 4e). Results from uniaxial compression testing indicated that achieving the same 20% deformation required a greater force in the glycation-treated tissue (Figure 4f). Additionally, the Young's modulus of the tissue significantly increased from 3.47 kPa to 7.84 kPa. Both mechanical characterizations indicate that glycation results in increased stiffness of ex vivo skin tissue. Therefore, we chose uniaxial compression testing as a primary indicator for analyzing the anti-glycation effects of SRFF in subsequent treatments.

## SRFF Demonstrates an Anti-Glycation Effect in Fibroblasts and ex vivo Specimens

We validated the anti-glycation effect of SRFF on fibroblasts, as illustrated in Figures 5. Our previous work confirmed that the concentrations of SRFF ranging from 0.25 to 10 mg/mL do not adversely affect fibroblast viability. Therefore, both 1 mg/mL and 10 mg/mL are considered safe concentrations for use.[35] When using SRFF on skin, the stratum corneum blocks its water-soluble components from penetrating effectively, and the solution struggles to stay on the skin long enough for lasting effects. Thus, iontophoresis and nanogel carriers were used to address skin glycation with SRFF.

GLA was used to induce glycation in ex vivo skin tissues, after which SRFF was applied for treatment. The experimental timeline is shown in Figure 6a. Increased yellowness was observed both visually and quantitatively with a chromameter, demonstrating that glycation of epidermal skin contributes to the appearance of skin yellowing (Figure 6b and Table 1). Following the application of SRFF/SRFF@HA nanogel, b* values decreased in both the topical and iontophoresis groups, and the iontophoresis group showed statistically significant differences compared to the control group. As shown in H&E staining results (Figure S4), noticeable pigment deposition can be observed in the skin tissue treated with GLA (as indicated by the dashed line box in the image). Alternatively, pigment deposition was mitigated to some extent after applying SRFF, in both the painting and iontophoresis group, particularly in the iontophoresis group.

Following SRFF/SRFF@HA nanogel application on the skin tissue surface, as presented in Figure 6c and d, the expression of CML in both the painting and iontophoresis group significantly decreased compared with the control group, suggesting a mitigation of glycation levels. Through the use of SRFF, these characteristics were alleviated, especially in the iontophoresis group. This indicates that SRFF plays a role in combating skin photoaging, with iontophoresis enhancing this effect due to increased transdermal SRFF delivery. In this study, the effect of SRFF on cellular tissue glycation primarily manifests as a reduction in CML expression. In the iontophoresis group, CML expression significantly decreased in both the epidermis and dermis, indicating that SRFF is effective in reducing CML in both layers and has penetrated deeply into the dermis to exert its effects. Moreover, SRFF slightly improved skin yellowing and melanin deposition.

Tissue stiffness due to glycosylation is crucial in diseases such as cancer and metabolic disorders. In metastatic colorectal cancer, fibroblasts increase tissue stiffness, promoting angiogenesis.[36] However, skin glycation remains unexplored. Notably, we observed tissue hardening from GLA through sensory perception, and instruments quantified this index. The results (Figure 6e) showed that after the application and iontophoresis of SRFF, the force required to compress the skin tissue and induce deformation was significantly reduced compared to the control group, decreasing from 17.94 gf (1 gf=0.0981 N) to 15.19 gf and 13.71 gf, respectively. Furthermore, the Young's modulus of the skin tissue decreased from 7.84 kPa to 7.60 kPa and 5.18 kPa, respectively, shown as Figure 6f. Notably, the group treated with SRFF demonstrated superior therapeutic effects, exhibiting statistically significant reductions in the minimum force

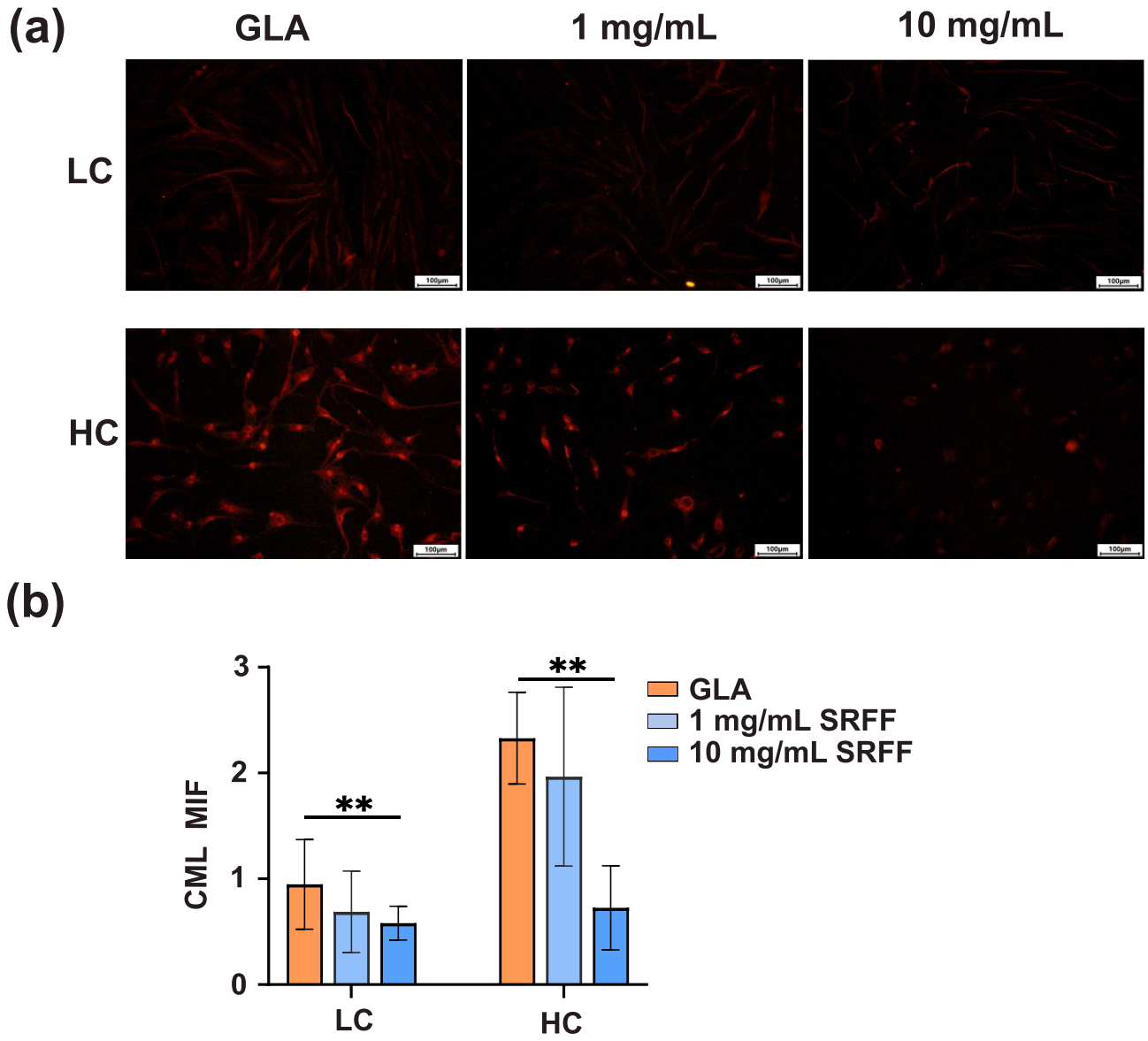


**Figure 5** SRFF was used to treat skin cell glycation. (**a**) CML (red) stained glycated fibroblasts treated by 10 mg/mL and 1 mg/mL SRFF solution (scale bar = 50 μm). (**b**) Relative quantification of CML expression level and comparison between GLA treatment group and SRFF treatment groups (** represents *P* <0.01 compared with the GLA group).

required for 20% deformation and Young's modulus compared to the control group. Thus, the SRFF reducing the stiffness of the glycation skin tissues.

## Discussion

The main components of SRFF, including amino acids, nucleotides, flavonoids, and polyphenols, generally carry a negative charge. Under the influence of the electric field, the free SRFF components can directly penetrate the stratum corneum into the skin tissue. Factors such as current density, concentration, and temperature impact the efficiency of drug delivery via iontophoresis.[37] Typically, the amount of drug permeation increases with higher current densities.[38] However, it is crucial that the current density does not exceed physiological thresholds to avoid causing pain. In dermatological applications,[36,39] current densities range widely from 0.1 to 4 mA/cm$^2$. Generally, several studies suggest that a current density of 0.5 mA /cm$^2$ yields effective results.[37,40,41] However, some researchers advocate using 0.2 mA / cm$^2$ as a safer alternative to 0.5 mA /cm$^2$, despite its lower efficiency.[38] Based on the equipment we utilized, a current

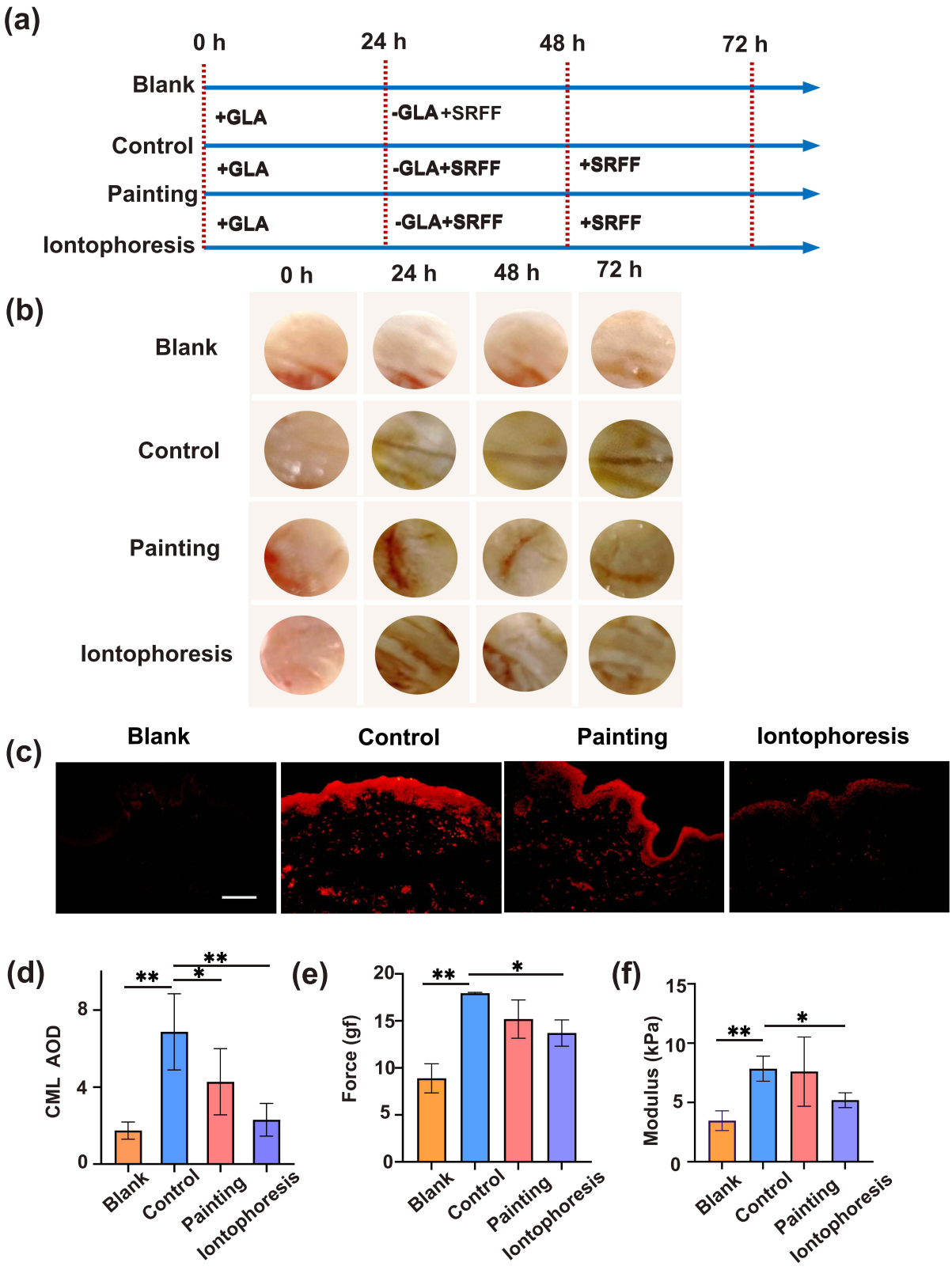


**Figure 6** SRFF was used to combat skin tissue glycation. (**a**) Timeline of establishing a skin glycation model and treatment. (**b**) Images of skin tissues from different time points in each group. (**c**) CML (red) and DAPI (blue) stained ex vivo skin tissues treated by SRFF solution (scale bar = 50 μm). (**d**) Relative quantification of CML expression level and comparison between different treatment groups (* and ** represents P <0.05 and P <0.01 compared with the control group, respectively). (**e**) and (**f**) The forces to achieve 20% strain and Young's modulus comparison among different treatment groups. Compared with Blank group (* and ** represents P <0.05 and P <0.01 compared with the control group, respectively).


https://doi.org/10.2147/IJN.S523731

**Table 1** B* Values at Different Time Points

| Groups | 0 h | 24 h | 48 h | 72 h |
|---|---|---|---|---|
| Blank | 25 ± 1.3 | 20 ± 2.1 | 24 ± 1.4 | 24 ± 1.6 |
| Control | 21 ± 2.5$^{ns}$ | 33 ± 4.4* | 35 ± 2.5 | 35 ± 1.5 |
| Painting | 23 ± 1.6$^{ns}$ | 32 ± 7.2* | 25 ± 2.1$^{\#\#}$ | 33 ± 1.7 |
| Iontophoresis | 24 ± 1.5$^{ns}$ | 34 ± 4.3* | 24 ± 2.5$^{\#\#}$ | 27 ± 2.5$^{\#\#}$ |

**Notes**: Compared with the blank group (0h): ns represents $P > 0.05$, * represents $P < 0.05$;Compared with the control group (24h): $^{\#\#}$represents $P < 0.01$.

**Abbreviations**: AGEs, advanced glycation end products; AFM, Atomic force microscope; DEGDA, di (ethylene glycol) diacrylate; DLS, dynamic light scattering; ECM extracellular matrix, FITC, fluorescein 5-isothiocyanate; GLA, DL-glyceraldehyde; HA, hyaluronic acid; HC, high concentration; HPLC-MS, high-performance liquid chromatography-mass spectrometry; LC, low concentration; MA, methacrylic anhydride; MWCO (molecular weight cut-off); NMR, nuclear magnetic resonance spectroscopy; PDI, polydispersity index; PET, polyethylene glycol terephthalate; ROS, reactive oxygen species; SRFF, Saccharomyces/rice ferment filtrate; SRFF@nanogel, SRFF-loaded nanogels; SEM, scanning electron microscope.

density of 0.6 to 1.6 mA/cm$^2$ for 25 minutes is deemed suitable for facial delivery and promotes transdermal permeation of macromolecules such as collagen (*M*w= 55 kDa).[26] Considering that the molecular weight of the main components of SRFF is smaller than that of collagen and prioritizing safety, we selected a current density of 0.6 mA /cm$^2$ for 25 minutes as the iontophoresis parameters.

At the chosen iontophoresis condition, HA nanogels cannot penetrate the stratum corneum and remain there, gradually releasing SRFF for sustained effects. These findings indicate that the loaded nanogels predominantly exert their therapeutic effects in a localized manner within the skin layers, minimizing systemic exposure and potential off-target effects. The retention of nanogels within the stratum corneum and epidermis for up to 5 days suggests a sustained local release profile, which could enhance treatment durability and reduce the need for frequent reapplication. However, the limited penetration beyond the epidermis also implies that delivery to deeper skin layers may be restricted, which might affect efficacy for targets located in the dermis or subcutaneous tissue. The reason for nanogels not penetrating deeper may be that the size of nanoparticles (approximately 55 nm) limits their transdermal ability. Studies have shown that nanoparticles smaller than 10 nm can passively penetrate the stratum corneum, while those larger than 20 nm can only penetrate through hair follicles. Nanogels with particle sizes with small size (<100 nm) are more difficultly in penetrate hair follicles than large ones (300 ~ 500 nm).[42] Additionally, since the ex vivo skin tissue used in the experiment was foreskin tissue, which lacks hair follicles, nanogels transdermal penetration is difficult. It is anticipated, based on previous studies,[43] that the remaining SRFF will be released upon complete degradation of the nanogel. Although it has been established that nanogels exhibit a certain degree of sustained release, the release rate within 24 hours is not sufficiently high, further optimization is necessary.

Although the short-term results with the SRFF-loaded HA nanogel combined with iontophoresis are promising, long-term in vivo studies are needed to evaluate the sustained efficacy, safety, and potential cumulative benefits of SRFF treatment. Additionally, optimizing iontophoresis parameters, such as current density, treatment duration, and frequency, could further improve delivery efficiency and enhance patient compliance. In future research on precision iontophoretic drug delivery, iontophoresis devices could enable personalized, real-time monitoring and treatment, thereby advancing practical applications in cosmetic dermatology and anti-aging treatments.

The relationship between glycation and aging has been extensively investigated.[44] Studies have indicated that with advancing age, the accumulation of AGEs in skin tissue, particularly within the dermal compartment, constitutes a significant factor contributing to visible skin aging and yellowing.[45] Nevertheless, the alterations in the mechanical properties of skin tissue as a result of glycation remain inadequately understood, despite their critical implications for diseases such as cancer and metabolic disorders, where fibroblast activity increases tissue stiffness and promotes angiogenesis.

There are multiple methods to measure skin stiffness, and a significant discrepancy of Young's modulus values was reported across different studies, from hundreds of Pa to hundreds of MPa.[46] These large discrepancies mainly arise from the testing methods themselves. Other contributing factors include variations in the species tested (humans, mice, or pigs). In our study, we measured the Young's modulus of human skin using both uniaxial compression tests and the AFM indentation method. Both methods revealed that GLA-induced glycation significantly increased tissue stiffness, while iontophoresis of SRFF reduced skin stiffness. Alongside the measurement of AGEs expression, mechanical data indicated effects on overall skin functionality. This multi-dimensional evaluation facilitates a more accurate determination of treatment efficacy.

But the Young's modulus obtained from uniaxial compression tests differed by three orders of magnitude from that obtained via AFM indentation. The differences between the two mechanical testing methods might stem from variations in the testing equipment and differences in measurement scales. AFM indentation experiments generally involve very small probes that measure local, surface-level stiffness, making this method particularly sensitive to the response of the skin's microstructure. In contrast, uniaxial compression experiments provide a macroscopic assessment of mechanical behavior, measuring how materials respond at larger strains and accounting for the material's nonlinear characteristics.

In fact, significant discrepancies in elastic modulus values are not unique to skin but are also observed in other soft tissues,[47] reflecting the inherent challenges in accurately measuring, analyzing, and interpreting the mechanical properties of these materials. While a definitive explanation for these variations remains lacking, it has been suggested that factors such as the testing method employed and the scale of the tissue sample examined play a crucial role in the measured modulus.[47,48]

ROS are critical participants in the glycation process. Antioxidants protect the structural integrity of proteins from damage and inhibit the highly reactive precursors of AGEs (carbonyl compounds) generated by the cleavage of sugar chains or lipid peroxidation. Neutralizing and scavenging free radicals, as well as reducing oxidative stress and ROS production, are essential methods for inhibiting the formation of AGEs.[3,49] There are flavonoids and polyphenols in the SRFF, which serve as antioxidants to help the skin mitigate free radical damage, thereby slowing down the glycation process. We have previously investigated the antioxidant capacity of SRFF in another study.[35] We evaluated intracellular ROS generation and observed that treatment with SRFF resulted in a concentration-dependent decrease in ROS levels.

Some natural compounds inhibit the formation of AGEs by competitively binding to the glycation sites on proteins, thus stabilizing the protein structure.[19] Among these, lysine and arginine residues are the most susceptible to glycation, due to sugars exhibiting higher affinity toward them.[50] Lysine and arginine residues are important components of SRFF, comprising 4.69% of its composition. Adenosine, also present in the SRFF composition, can stimulate collagen production in the dermis via the A2 adenosine receptor subtype.[51]

To further verify the binding between SRFF and AGEs, we selected several compounds from the SRFF composition and conducted molecular docking simulations to investigate their molecular interactions (detailed simulation procedures are provided in the supplementary materials). Carnosine is known to exhibit good anti-glycation properties.[22,52] Carnosine, present in SRFF at a concentration of 0.122 mg/g, was found to bind AGEs through visible hydrogen bonds and strong electrostatic interactions. Furthermore, the hydrophobic pockets of AGEs were successfully occupied by carnosine. The carnosine-AGE complex exhibited a low binding energy of −4.97 kcal/mol, indicating a highly stable interaction (Figure S5a). We also examined the binding energies of DL-arginine (4.279 mg/g) and a lysine derivative, N-6-(Carboxymethyl)-L-lysine (1.056 mg/g), with AGEs. They yielded binding energies of −5.469 kcal/mol (Figure S5b) and −8.368 kcal/mol (Figure S5c), respectively, both demonstrating strong binding affinity.

Overall, SRFF is a mixture of bioactive compounds that may mitigate skin glycation effects by antioxidant activity, competitively binding to AGEs, and promoting collagen secretion. Further research is needed to identify the specific active substances responsible for this effect and elucidate the underlying mechanisms by isolating components of the SRFF mixture and performing genetic or protein sequencing.

## Conclusion

In summary, SRFF was utilized for anti-glycation through iontophoresis, effectively reducing the generation of AGEs and tissue stiffness. The anti-glycation effects of SRFF were observed at both cellular and ex vivo skin tissue levels,

likely attributed to the antioxidant components in SRFF and constituents that competitively bind to cross-linking sites of AGEs. A nano-scaled HA hydrogel was prepared for SRFF encapsulation, residing in the epidermis and gradually releasing into glycated skin. Iontophoresis technology effectively addressed the challenges of SRFF's high hydrophilicity and poor transdermal permeability, significantly enhancing transdermal quantity and efficiency. The combination of HA nanogel and iontophoresis represents an effective drug delivery method.

However, this study is limited by the lack of long-term in vivo data to confirm sustained efficacy and safety, as well as a detailed mechanistic understanding of SRFF's interactions with glycation pathways at the molecular level. Future research should focus on optimizing iontophoresis parameters, exploring flexible and wearable iontophoresis devices for personalized skincare applications.

## Acknowledgments

This work was supported by grants from National Key Research and Development Program of China, 2022YFB3804701, and National Natural Science Foundation of China (Nos. 82173441).

## Disclosure

The authors report no conflicts of interest in this work.

## References

1. Twarda-Clapa A, Olczak A, Białkowska AM, et al. Advanced glycation end-products (ages): formation, chemistry, classification, receptors, and diseases related to AGEs. *Cells*. 2022;11(8):1312. doi:10.3390/cells11081312
2. Wahhab R, Sanders M, Kokikian N, et al. Clinical consequences of age-related skin barrier dysfunction. part i. structural, molecular and physiologic changes with cutaneous aging. *J Am Acad Dermatol*. 2024. doi:10.1016/j.jaad.2024.08.044
3. Wan L, Bai X, Zhou Q, et al. The advanced glycation end-products (AGEs)/ROS/NLRP3 inflammasome axis contributes to delayed diabetic corneal wound healing and nerve regeneration. *Int J Biol Sci*. 2022;18(2):809–825. doi:10.7150/ijbs.63219
4. Chen C, Zhang JQ, Li L, et al. Advanced glycation end products in the skin: molecular mechanisms, methods of measurement, and inhibitory pathways. *Front Med*. 2022;9:837222. doi:10.3389/fmed.2022.837222
5. Wang L, Jiang Y, Zhao C. The effects of advanced glycation end-products on skin and potential anti-glycation strategies. *Exp Dermatol*. 2024;33 (4):e15065. doi:10.1111/exd.15065
6. Yan SF, Ramasamy R, Schmidt AM. Mechanisms of disease: advanced glycation end-products and their receptor in inflammation and diabetes complications. *Nat Clin Pract Endocrinol Metab*. 2008;4(5):285–293. doi:10.1038/ncpendmet0786
7. Reddy VP, Aryal P, Darkwah EK. Advanced glycation end products in health and disease. *Microorganisms*. 2022;10(9):1848. doi:10.3390/microorganisms10091848
8. Gautieri A, Passini FS, Silván U, et al. Advanced glycation end-products: mechanics of aged collagen from molecule to tissue. *Matrix Biol*. 2017;59:95–108. doi:10.1016/j.matbio.2016.09.001
9. Gill V, Kumar V, Singh K, et al. Advanced glycation end products (AGEs) may be a striking link between modern diet and health. *Biomolecules*. 2019;9(12):888. doi:10.3390/biom9120888
10. Danby FW. Nutrition and aging skin: sugar and glycation. *Clin Dermatol*. 2010;28(4):409–411. doi:10.1016/j.clindermatol.2010.03.018
11. Oh S, Rho NK, Byun KA, et al. Combined treatment of monopolar and bipolar radiofrequency increases skin elasticity by decreasing the accumulation of advanced glycated end products in aged animal skin. *Int J Mol Sci*. 2022;23(6):2993. doi:10.3390/ijms23062993
12. Xie Y, Ye J, Ouyang Y, et al. Microneedle-assisted topical delivery of idebenone-loaded bioadhesive nanoparticles protect against uv-induced skin damage. *Biomedicines*. 2023;11(6):1649. doi:10.3390/biomedicines11061649
13. Chakraborty R, Afrose N, Kuotsu K, et al. Novel synergistic approaches of protein delivery through physical enhancement for transdermal microneedle drug delivery: a review. *J Drug Deliv Sci Technol*. 2023;84:104467. doi:10.1016/j.jddst.2023.104467
14. Zheng W, Li H, Go Y, et al. Research advances on the damage mechanism of skin glycation and related inhibitors. *Nutrients*. 2022;14(21):4588. doi:10.3390/nu14214588
15. Brings S, Fleming T, Freichel M, Muckenthaler MU, Herzig S, Nawroth PP. Dicarbonyls and advanced glycation end-products in the development of diabetic complications and targets for intervention. *Int J Mol Sci*. 2017;18(5):984. doi:10.3390/ijms18050984
16. Thornalley PJ. Use of aminoguanidine (Pimagedine) to prevent the formation of advanced glycation endproducts. *Arch Biochem Biophys*. 2003;419 (1):31–40. doi:10.1016/j.abb.2003.08.013
17. Freedman BI, Wuerth JP, Cartwright K, et al. Design and baseline characteristics for the aminoguanidine Clinical Trial in Overt Type 2 Diabetic Nephropathy (ACTION II). *Control Clin Trials*. 1999;20(5):493–510. doi:10.1016/S0197-2456(99)00024-0
18. Jangde N, Ray R, Rai V. RAGE and its ligands: from pathogenesis to therapeutics. *Crit Rev Biochem Mol Biol*. 2020;55(6):555–575. doi:10.1080/10409238.2020.1819194
19. Song Q, Liu J, Dong L, et al. Novel advances in inhibiting advanced glycation end product formation using natural compounds. *Biomed Pharmacother*. 2021;140:111750. doi:10.1016/j.biopha.2021.111750
20. Ar MM, Hongsprabhas P, Thottiam R. In vitro and in vivo inhibition of maillard reaction products using amino acids, modified proteins, vitamins, and genistein: a review. *J Food Biochem*. 2019;43(12):e13089. doi:10.1111/jfbc.13089
21. Khan M, Liu H, Wang J, et al. Inhibitory effect of phenolic compounds and plant extracts on the formation of advance glycation end products: a comprehensive review. *Food Res Int*. 2020;130:108933. doi:10.1016/j.foodres.2019.108933

22. Bai D, Wang Z, Xie L, et al. Topical transdermal administration of supramolecular self-assembled carnosine for anti-melanin and anti-aging. *Adv Healthc Mater*. 2024;13. doi:10.1002/adhm.202401960
23. Chen A, Luo Y, Xu J, et al. Latest on biomaterial-based therapies for topical treatment of psoriasis. *J Mater Chem B*. 2022;10(37):7397–7417. doi:10.1039/D2TB00614F
24. Gupta DK, Ahad A, Aqil M, et al. Iontophoretic drug delivery: concepts, approaches, and applications. *Adv Modern Approaches Drug Del*. 2023:515–546.
25. Gaikwad SS, Zanje AL, Somwanshi JD. Advancements in transdermal drug delivery: a comprehensive review of physical penetration enhancement techniques. *Int J Pharm*. 2024;652:123856. doi:10.1016/j.ijpharm.2024.123856
26. Song D, Tao W, Tang Z, Hu X. Conductive electronic skin coupled with iontophoresis for sensitive skin treatment. *J Drug Deliv Sci Technol*. 2024;95:105650. doi:10.1016/j.jddst.2024.105650
27. Mailloux RJ, Bériault R, Lemire J, et al. The tricarboxylic acid cycle, an ancient metabolic network with a novel twist. *PLoS One*. 2007;2(8):e690. doi:10.1371/journal.pone.0000690
28. Yang F, Zhou Z, Guo M, et al. The study of skin hydration, anti-wrinkles function improvement of anti-aging cream with alpha-ketoglutarate. *J Cosmet Dermatol*. 2022;21(4):1736–1743. doi:10.1111/jocd.14635
29. Yang C, Li C, Zhang P, Wu W, Jiang X. Redox responsive hyaluronic acid nanogels for treating RHAMM (CD168) over-expressive cancer, both primary and metastatic tumors. *Theranostics*. 2017;7(6):1719–1734. doi:10.7150/thno.18340
30. Yuliarto B, Septina W, Fuadi K, Fanani F, Muliani L. Synthesis of nanoporous tio2 and its potential applicability for dye-sensitized solar cell using antocyanine black rice. *Adv Mater Sci Eng*. 2010;1:789541.
31. Semwal R, K JS, Semwal R, et al. Health benefits and limitations of rutin-A natural flavonoid with high nutraceutical value. *Phytochem Lett*. 2021;46:119–128. doi:10.1016/j.phytol.2021.10.006
32. M SA, A AT, M RM, et al. Determination of total flavonoid content by aluminum chloride assay: a critical evaluation. *Lwt*. 2021;150:111932. doi:10.1016/j.lwt.2021.111932
33. Gaffney DO, Jennings EQ, Anderson CC, et al. Non-enzymatic lysine lactoylation of glycolytic enzymes. *Cell Chem Biol*. 2020;27(2):206–213. doi:10.1016/j.chembiol.2019.11.005
34. Laughlin T, Tan Y, Jarrold B, et al. Autophagy activators stimulate the removal of advanced glycation end products in human keratinocytes. *J Eur Acad Dermatol Venereol*. 2020;34(S3):12–18. doi:10.1111/jdv.16453
35. Li Y, Guo M, Li L, Yang F, Xiong L. Effects of rice fermentation and its bioactive components on UVA-induced oxidative stress and senescence in dermal fibroblasts. *Photochem Photobiol*. 2025;101(2):392–403. doi:10.1111/php.14003
36. Pikal MJ. The role of electroosmotic flow in transdermal iontophoresis. *Adv Drug Deliv Rev*. 2001;46(1–3):281–305. doi:10.1016/S0169-409X(00)00138-1
37. Nugroho AK, Li G, Grossklaus A, et al. Transdermal iontophoresis of rotigotine: influence of concentration, temperature and current density in human skin in vitro. *J Control Release*. 2004;96(1):159–167. doi:10.1016/j.jconrel.2004.01.012
38. Prasad R, Koul V, Anand S. Biophysical assessment of DC iontophoresis and current density on transdermal permeation of methotrexate. *Int J Pharm Investig*. 2011;1(4):234. doi:10.4103/2230-973X.93011
39. Anderson CR, Morris RL, Boeh SD, et al. Effects of iontophoresis current magnitude and duration on dexamethasone deposition and localized drug retention. *Phys Ther*. 2003;83(2):161–170. doi:10.1093/ptj/83.2.161
40. Saepang K, Li SK, Chantasart D. Effect of pulsed direct current on iontophoretic delivery of pramipexole across human epidermal membrane in vitro. *Pharm Res*. 2021;38(7):1187–1198. doi:10.1007/s11095-021-03055-3
41. Zheng Y, Ye R, Gong X, et al. Iontophoresis-driven microneedle patch for the active transdermal delivery of vaccine macromolecules. *Microsyst Nanoeng*. 2023;9(1):35. doi:10.1038/s41378-023-00515-1
42. Tiwari N, Osorio-Blanco ER, Sonzogni A, et al. Nanocarriers for skin applications: where do we stand? *Angew Chem Int Ed*. 2022;61(3):e202107960. doi:10.1002/anie.202107960
43. Wang R, Wang X, Zhan Y, et al. A dual network hydrogel sunscreen based on poly-γ-glutamic acid/tannic acid demonstrates excellent anti-UV, self-recovery, and skin-integration capacities. *ACS Appl Mater Interfaces*. 2019;11(41):37502–37512. doi:10.1021/acsami.9b14538
44. Shin ES, Sang Park Y, Nam SH. Non-invasive assessments of the advanced glycation end products in human skin using reflectance NIR spectroscopy. *2019 41st Annual International Conference of the IEEE Engineering in Medicine and Biology Society (EMBC)*. 2019. 23–27; Berlin, Germany: IEEE.
45. Zhang J, Reinhart-King CA. Targeting tissue stiffness in metastasis: mechanomedicine improves cancer therapy. *Cancer Cell*. 2020;37(6):754–755. doi:10.1016/j.ccell.2020.05.011
46. Wahlsten A, Stracuzzi A, Lüchtefeld I, et al. Multiscale mechanical analysis of the elastic modulus of skin. *Acta Biomater*. 2023;170:155–168. doi:10.1016/j.actbio.2023.08.030
47. McKee CT, Last JA, Russell P, Murphy CJ. Indentation versus tensile measurements of Young's modulus for soft biological tissues. *Tissue Eng Part B Rev*. 2011;17(3):155–164. doi:10.1089/ten.teb.2010.0520
48. Graham HK, McConnell JC, Limbert G, Sherratt MJ. How stiff is skin? *Exp Dermatol*. 2019;28(Suppl 1):4–9. doi:10.1111/exd.13826
49. Guo J, Huang X, Dou L, et al. Aging and aging-related diseases: from molecular mechanisms to interventions and treatments. *Signal Transduct Target Ther*. 2022;7(1):391. doi:10.1038/s41392-022-01251-0
50. Collier TA, Nash A, Birch HL, et al. Intra-molecular lysine-arginine derived advanced glycation end-product cross-linking in Type I collagen: a molecular dynamics simulation study. *Biophys Chem*. 2016;218:42–46. doi:10.1016/j.bpc.2016.09.003
51. Feoktistov I, Biaggioni I, Cronstein BN. Adenosine receptors in wound healing, fibrosis and angiogenesis. *Exp Pharmacol*. 2009;193:383–397.
52. Reddy VP, Garrett MR, Perry G, Smith MA. Carnosine: a versatile antioxidant and antiglycating agent. *Sci Aging Knowl Environ*. 2005;2005(18):pe12. doi:10.1126/sageke.2005.18.pe12